Journal of Materials Science & Technology 93 (2021) 28–32

Contents lists available at ScienceDirect

Journal of Materials Science & Technology

journal homepage: www.elsevier.com/locate/jmst

Research Article

Microwave dielectric high-entropy ceramic $Li(Gd_{0.2}Ho_{0.2}Er_{0.2}Yb_{0.2}Lu_{0.2})GeO_4$ with stable temperature coefficient for low-temperature cofired ceramic technologies

Huaicheng Xiang[a,b], Lei Yao[a,*], Junqi Chen[c], Aihong Yang[c], Haitao Yang[a,*], Liang Fang[c,*]

[a] Shenzhen Key Laboratory of Special Functional Materials, Shenzhen Engineering Laboratory for Advanced Technology of Ceramics, Guangdong Research Center for Interfacial Engineering of Functional Materials, College of Materials Science and Engineering, Shenzhen University, Shenzhen 518060, China
[b] Key Laboratory of Optoelectronic Devices and Systems of Ministry of Education and Guangdong Province, College of Physics and Optoelectronic Engineering, Shenzhen University, Shenzhen 518060, China
[c] Guangxi Key Laboratory of Optical and Electronic Materials and Devices, College of Materials Science and Engineering, Guilin University of Technology, Guilin 541004, China

ARTICLE INFO

Article history:
Received 18 February 2021
Revised 18 March 2021
Accepted 20 March 2021
Available online 12 May 2021

Keywords:
High-entropy ceramic
Octahedral distortion
Microwave dielectric properties
Stable τ_f

ABSTRACT

High-entropy ceramics are new single-phase materials with at least four cation or anion types. Their large configurational entropy is believed to enhance the simultaneous solubility of many components, which can be used to optimize certain properties. In this work, a high-entropy oxide, $Li(Gd_{0.2}Ho_{0.2}Er_{0.2}Yb_{0.2}Lu_{0.2})GeO_4$ (LRG) was explored as a microwave dielectric ceramic for low-temperature cofired ceramic technologies. The LRG high-entropy ceramic with an olivine structure formed in the sintering temperature range of 1020–1100 °C. The minimal distortion (5×10^{-4}) of the [RO_6] octahedron led to a stable temperature coefficient of resonant frequency (τ_f) of –5.3 to –2.9 ppm/°C. Optimal microwave dielectric properties were achieved in the high-entropy ceramics at 1080 °C for 4 h with a relative density of 94.9%, a relative permittivity (ε_r) of 7.2, and a quality factor ($Q\times f$) of 29000 GHz (at 15.3 GHz). For low-temperature cofired ceramic technology applications, the sintering temperature of the LRG high-entropy ceramic was reduced to 900 °C by the addition of 3 wt% H_3BO_3, which exhibited outstanding microwave dielectric properties ($\varepsilon_r = 7.6$, $Q\times f = 11700$ GHz, and $\tau_f = -7.4$ ppm/°C) and a good chemical compatibility with silver.

1. Introduction

The new generation of wireless systems (5 G and 6 G) offer a faster and more reliable broadband access, with a greater capacity and a shorter latency. These properties require microwave dielectric materials with a low sintering temperature (< 960 °C), low dielectric loss (i.e., high quality factor $Q\times f$, tan δ =1/Q < 0.001), low permittivity (ε_r < 15), and a near-zero and stable temperature coefficient of resonance frequency (–10 ppm/°C ≤ τ_f ≤ +10 ppm/°C) to ensure high-quality component fabrication [1-3]. Few microwave dielectric ceramics meet the above performance requirements. Significant progress has been made in the development of new microwave dielectric ceramics with a low permittivity and high quality factor, but the major limiting factor remains the unstable temperature coefficient of resonance frequency. Olivine-structured microwave dielectric ceramics have been studied extensively as a representative material, and include A_2BO_4 (A = Ca, Mg; B = Si, Ge), Li_2MGeO_4 (M = Zn, Mg), $LiYGeO_4$, and $LiInSiO_4$ [4-11]. A low relative permittivity is the main feature of the olivine microwave dielectric ceramics, which makes them potential candidates for the new generation of communication devices. However, the high sintering temperature and large negative τ_f of the olivine-structured ceramics are impractical in applications that demand low-temperature cofired ceramic (LTCC) technology [12, 13].

As an emerging concept in the field of metallic alloys, high-entropy metal alloys (HEAs) have aroused extensive research interest. Since the invention of HEAs in 2004, intensive research on HEAs has produced interesting results, such as an enhanced hardness and strength [14-16]. High-entropy ceramics, by analogy to HEAs, are an emerging class of solid–solutions that are composed of a large number of species. High-entropy ceramics are single-phase ceramics with at least four types of cations or anions. Because the minimization of Gibbs free energy ($G = H–TS$, where H is enthalpy, S is entropy, and T is temperature) controls the ther-

* Corresponding authors.
E-mail addresses: lyao@szu.edu.cn (L. Yao), yanght63@szu.edu.cn (H. Yang), fangliangg1001@aliyun.com (L. Fang).

https://doi.org/10.1016/j.jmst.2021.03.057
1005-0302/

modynamic stability of the material, high-entropy materials with a large S can be more stable at high temperatures [17-19]. A high entropy produces attractive qualities, including a preference for single-phase solid–solutions with simple crystal structures, sluggish kinetics, lattice distortions, and a collection of properties that exceeds those of the constituent materials [20, 21]. High-entropy strategies have been applied in various fields, including thermoelectricity, catalysis, and superionic conductors. However, limited research on high-entropy ceramics has been reported in the field of microwave dielectrics. Recent works have indicated that the crystal structure stability in microwave dielectric ceramics has an important correlation with τ_f, which provides a structural basis to introduce the high-entropy concept into microwave dielectric ceramics.

The crystal structures of the major phases of $LiREGeO_4$ (RE = La–Lu) can be classified into three groups: hexagonal (apatite-type), tetragonal, and orthorhombic (olivine-type) [22], which provides a basis for the design of high-entropy ceramics. Orthorhombic olivine possesses a small unit cell volume and an oxygen octahedron structure, which is more favorable to regulate the microwave dielectric properties. Therefore, we prepared a $Li(Gd_{0.2}Ho_{0.2}Er_{0.2}Yb_{0.2}Lu_{0.2})GeO_4$ (LRG) high-entropy ceramic through a solid-state reaction route and investigated the relationship between its structure and its microwave dielectric properties. It is hoped that these high-entropy research strategies and results can provide important theoretical and practical guidance for the high-performance design of microwave dielectric ceramics.

2. Experimental

High-entropy oxide ceramic LRG was synthesized by a solid-state reaction process, using high-purity (> 99%) raw powders of Li_2CO_3, Gd_2O_3, Ho_2O_3, Er_2O_3, Yb_2O_3, Lu_2O_3, and GeO_2, where Gd_2O_3:Ho_2O_3:Er_2O_3:Yb_2O_3:Lu_2O_3 = 1:1:1:1:1 with an equimolar composition. The powders were placed in a zirconia ceramic jar and milled in a high-energy planetary ball mill (PM100, Retsch, Germany) with ethanol and zirconia balls for 6 h at 300 rpm. The ball-milled slurry was dried in an oven at 120 °C for 24 h, whereafter the powder was ground in an agate mortar, placed in an alumina crucible and calcined at 950 °C for 6 h at 5 °C/min. The calcined powder was ball-milled a second time, 5 wt% polyvinyl alcohol aqueous solution (PVA) was added as a binder, and the powder was pressed into 5-mm-high cylinders with a 10-mm diameter. The LRG green samples were annealed at 600 °C for 10 h at 1 °C/min to remove the PVA binder, and sintered at 1020–1100 °C for 6 h to measure the microwave dielectric properties. To reduce the sintering temperature and cofire with Ag, the calcined LRG powders were ball-milled with 3 wt.% H_3BO_3 for 6 h. The H_3BO_3-doped LRG samples were sintered at 860−920 °C for 4 h.

X-ray diffraction (XRD) analysis was performed on the prepared ceramics using a D8 Advance diffractometer (Bruker AXS, WI, USA) with a Cu–Kα line as radiation source. The resulting diffraction patterns were refined using FULLPROF software [23]. The ceramic microstructures were examined by scanning electron microscopy (SEM, SU-70, Hitachi, Japan). The Archimedes method was used to measure the apparent density. Hakki and Coleman's method was used to measure the ε_r and $Q\times f$ values with a vector network analyzer (10 MHz-20 GHz, ZVB20, Rohde & Schwarz, Germany) in TE_{011} mode [24]. The τ_f values in the range of 25–85 °C were calculated from $\tau_f=(f_{85}-f_{25})/[f_{25}(T_{85}-T_{25})]$ (where f_{25} and f_{85} denote the resonant frequencies at 25 °C and 85 °C).

3. Results and discussion

Fig. 1(a) shows the XRD patterns of the high-entropy LRG powder compared with the $LiGdGeO_4$ and $LiHoGeO_4$. The crystal structures of the major phase of $LiGdGeO_4$ and $LiHoGeO_4$ were classified into two groups: tetragonal for $LiGdGeO_4$, and orthorhombic (olivine type) for $LiHoGeO_4$. LRG high-entropy ceramics have the same structure (space group: *Pnma*, 62) as $LiHoGeO_4$. After annealing at 1020 to 1100 °C for 4 h in air, the XRD patterns showed no evidence of phase decomposition or transformation, which indicates that the high-entropy phase $Li(Gd_{0.2}Ho_{0.2}Er_{0.2}Yb_{0.2}Lu_{0.2})GeO_4$ is thermally stable up to 1100 °C. Rietveld refinement of XRD data for the LRG high-entropy ceramic that was sintered at 1060 °C for 4 h was conducted by using FULLPROF software (Fig. 1(b)). Good agreement resulted between the calculated and measured patterns with low values of R_{exp} = 6.15% and R_{wp} = 4.01% (Fig. 1(b)). The calculated lattice parameters are a = 11.0481 Å, b = 6.3174 Å, and c = 5.2062 Å for LRG. The lattice parameters and structures of the $LiRGeO_4$ (R = Gd, Ho, Er, Yb, Lu) system are summarized in Table 1. The LRG high-entropy ceramic exhibits a higher unit cell volume than other ceramics with an orthorhombic olivine structure, and five component elements (Gd, Ho, Er, Yb, and Lu) occupy the R sites evenly and randomly (Fig. 1(c)). The [LiO_6] and [RO_6] octahedra and [GeO_4] tetrahedron compose the crystal structure cell of the LRG high-entropy ceramic. In the $Li(Gd_{0.2}Ho_{0.2}Er_{0.2}Yb_{0.2}Lu_{0.2})GeO_4$ structure, the [RO_6] octahedra are linked by corner-sharing, and the [GeO_4] tetrahedra are isolated from each other. Each [RO_6] octahedron is connected with two adjacent [GeO_4] tetrahedra in the form of edge- and corner-sharing, and each Li atom is surrounded by six O atoms.

Grain growth is one of the most important factors for densification during sintering. Fig. 2 shows the densities and SEM images of the LRG high-entropy ceramic as a function of sintering temperature. The relative density increased with sintering temperature to 1080 °C, then decreased slightly because of overheating, which corresponded to the SEM image in the inset of Fig. 2. According to the calculated density (5.399 g/cm^3), the maximum relative density of LRG reaches 94.9%. LRG high-entropy ceramic densification was related positively to the sintering temperature. Some pores were visible at 1040 °C, and when the sintering temperature increased to 1080 °C, the LRG high-entropy ceramic exhibited a relatively dense microstructure with few visible pores.

Fig. 3(a) shows the change in ε_r of the LRG high-entropy ceramic as a function of sintering temperature. The ε_r of the LRG high-entropy ceramic increased gradually from 6.1 to 7.2 and then decreased to 7.1 with an increase in sintering temperature. The trend in ε_r of the LRG high-entropy ceramic was like that of the relative density, which indicates that density is important in the permittivity. According to the Bosman–Havinga equation ($\varepsilon_{corr.} = \varepsilon_r$ (1+1.5p)) [25, 26], the porosity in the sintered ceramics influences the ε_r. p and $\varepsilon_{corr.}$ are the fractional porosity and the corrected permittivity, respectively. The $\varepsilon_{corr.}$ is 7.74 for the LRG high-entropy ceramic sintered at 1080 °C. In the microwave region, the permittivity is affected by ionic polarizability. Shannon proposed that the molecular polarizability (α) of the compounds may be estimated by summing α of the constituent ions [27]. For $Li(Gd_{0.2}Ho_{0.2}Er_{0.2}Yb_{0.2}Lu_{0.2})GeO_4$:

$$\alpha_{LRG} = \alpha_{Li^+} + 0.2 \times \left(\alpha_{Gd^{3+}} + \alpha_{Ho^{3+}} + \alpha_{Er^{3+}} + \alpha_{Yb^{3+}} + \alpha_{Lu^{3+}}\right) + 4\alpha_{O^{2-}} = 14.74 Å^3 \quad (1)$$

where the ionic polarizabilities of Li^+, Gd^{3+}, Ho^{3+}, Er^{3+}, Yb^{3+}, Lu^{3+}, and O^{2-} are 1.20 Å^3, 4.37 Å^3, 3.97 Å^3, 3.81 Å^3, 3.58 Å^3, 3.64 Å^3, and 2.01 Å^3, respectively [27]. Based on the Clausius–Mosotti (C–M) equation, the calculated theoretical permittivity ($\varepsilon_{th.}$) is [28, 29]:

$$\varepsilon_{th.} = \frac{3V + 8\pi\alpha}{3V - 4\pi\alpha} \quad (2)$$

where V is the cell volume (363.3681/4 = 90.84 Å^3). The calculated permittivity is 7.37, which is close to the measured value (~7.2).

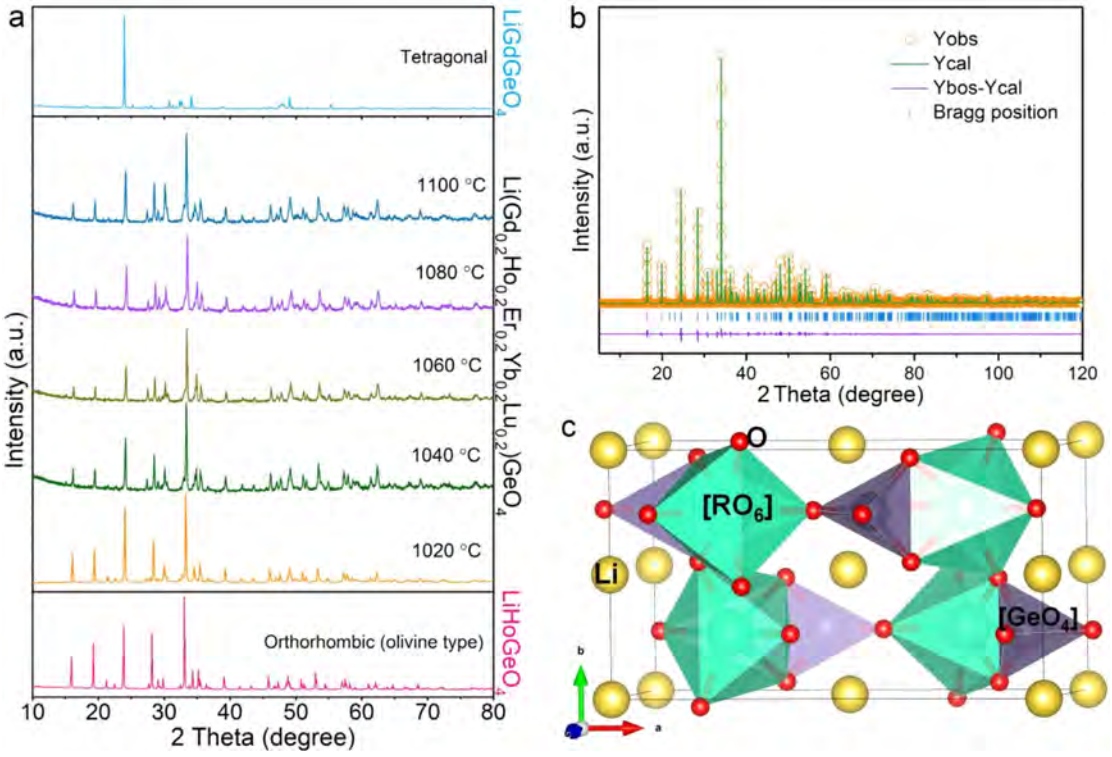

Fig. 1. (a) XRD patterns of LRG high-entropy ceramic at different sintering temperatures. (b) Rietveld refinement of LRG high-entropy ceramic sintered at 1060 °C for 4 h. (c) Schematic of crystal structure of LRG high-entropy ceramic.

Table 1
Lattice parameters, cell volumes, and structures of Li*R*GeO$_4$ (*R* = Gd, Ho, Er, Yb, Lu).

Material	*a* (Å)	*b* (Å)	*c* (Å)	*V* (Å^3)	Structure	Refs.
$LiGdGeO_4$	7.30	7.30	9.61	512	Tetragonal	[22]
$LiHoGeO_4$	11.10	6.31	5.07	353	Orthorhombic	[22]
$LiErGeO_4$	11.10	6.33	5.04	352	Orthorhombic	[22]
$LiYbGeO_4$	10.94	6.25	5.02	343	Orthorhombic	[22]
$LiLuGeO_4$	11.1401	6.3333	5.0656	357.4190	Orthorhombic	This work
$Li(Gd_{0.2}Ho_{0.2}Er_{0.2}Yb_{0.2}Lu_{0.2})GeO_4$	11.0481	6.3174	5.2062	363.3681	Orthorhombic	This work

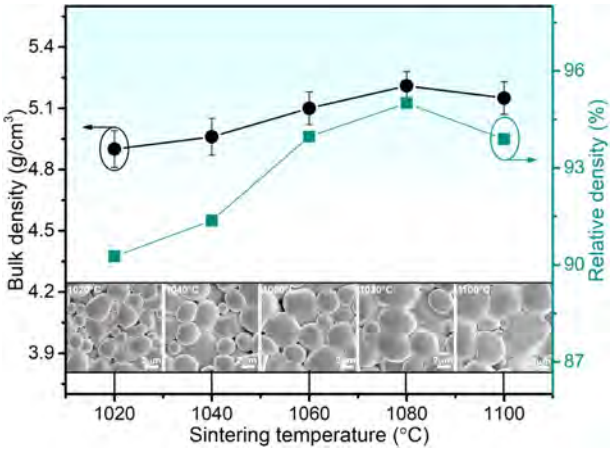

Fig. 2. Variation of bulk density and relative density as a function of sintering temperature, and SEM images of LRG high-entropy ceramic sintered at different temperatures.

The good agreement between the calculated and measured permittivity means that the C–M equation may be useful to predict the permittivity of novel high-entropy ceramics whose permittivity has not been measured.

Fig. 3(b) shows the $Q\times f$ values of the LRG high-entropy ceramic that was sintered at various temperatures. Like the dependence of relative density and permittivity on sintering temperature, the $Q\times f$ of the LRG high-entropy ceramic increased to a maximum of 29000 GHz at 15.3 GHz after sintering at 1080 °C for 4 h, and then decreased. The increase in $Q\times f$ value is attributed to the decrease in porosity. A further increase in sintering temperature to 1100 °C led to abnormal grain growth and the re-emergence of pores, which reduced the $Q\times f$ value.

As shown in Fig. 3(c), the dependence of the τ_f on the sintering temperature is less sensitive than that of other microwave dielectric parameters. The τ_f values of the LRG high-entropy ceramic changed from −5.3 to −2.9 ppm/°C when the sintering temperature increased from 1020 °C to 1100 °C, which indicates that the temperature stability of the LRG high-entropy ceramic system was outstanding. The τ_f of most microwave dielectric ceramics is affected by the ceramic structure, and especially by the distortion of the oxygen octahedron [30-34]. For LRG high-entropy ceramics, the five Gd^{3+}, Ho^{3+}, Er^{3+}, Yb^{3+}, and Lu^{3+} cations jointly occupy the position of the [RO_6] octahedron, which affects the oxygen octahedron distortion. The calculated octahedral distortion ($\Delta_{octa.}$) is [35]:

$$\Delta_{octa.} = \frac{1}{6}\sum\left(\frac{R_{i-o} - R_{av.}}{R_{av.}}\right)^2 \quad (3)$$

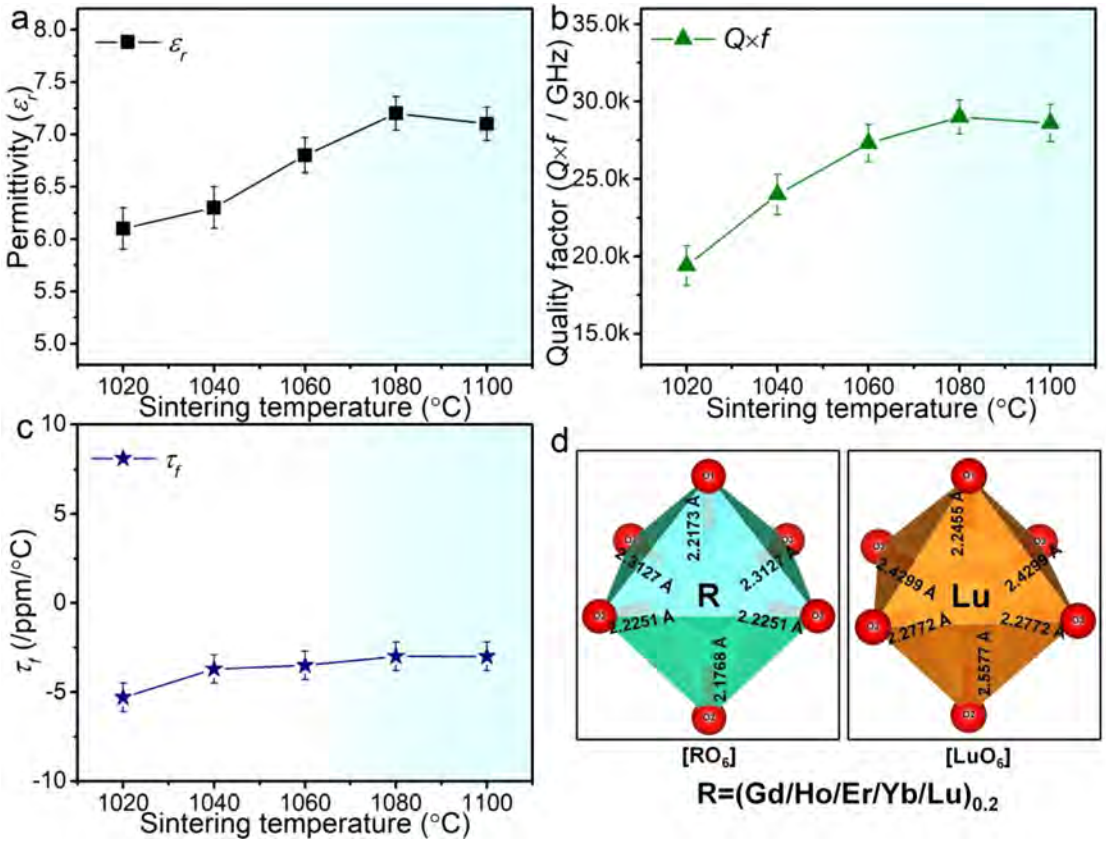

Fig. 3. Variation in (a) ε_r, (b) $Q\times f$, and (d) τ_f of LRG high-entropy ceramic as a function of sintering temperature. (d) Schematic of change in oxygen octahedron of LRG and $LiLuGeO_4$.

Table 2
The τ_f and oxygen octahedron information of Li-containing olivine microwave dielectric ceramics.

Ceramics	Crystal structure	oxygen octahedron	Type of bonds	Bond length (Å)	Octahedral distortion ($\Delta_{octa.}$)	τ_f (ppm/°C)	Refs.
$LiRGeO_4$	Olivine	$[RO]_6$	R-O1	2.2173	5×10^{-4}	-	This
		octahedron	R-O2	2.1768		2.9	work
			R-O3 × 2	2.3127			
			R-O3 × 2	2.2251			
$LiLuGeO_4$	Olivine	$[LuO]_6$	Lu-O1	2.2455	2.2×10^{-3}	-	This
		octahedron	Lu-O2	2.5577		17.9	work
			Lu-O3 × 2	2.4299			
			Lu-O3 × 2	2.2772			
$LiYGeO_4$	Olivine	$[YO]_6$ octahedron	/	/	/	-27.7	[10]
$LiYbSiO_4$	Olivine	$[YbO]_6$ octahedron	/	/	7.5×10^{-4}	+4.52	[39]
Li_2ZnGeO_4	Olivine	/	/	/	/	-60.6	[9]
Li_2MgGeO_4	Olivine	/	/	/	/	-70.4	[9]

where $R_{i\text{-}O}$ is the bond length of atom i and O, and $R_{av.}$ is the average bond length. The oxygen octahedral information of the LRG high-entropy ceramic is shown in Fig. 3(d) and Table 2. To explain the effect of oxygen octahedral distortion on τ_f, we investigated the $LiLuGeO_4$ ceramic structure and properties (Fig. S1 and Table S1, Supporting Information). The small distortion of the oxygen octahedron indicates that the structure is stable. Macroscopically, a slight displacement of the resonance peak results, that is, the temperature coefficient of the resonance frequency is close to zero. The $[RO_6]$ octahedron shows minimal distortion (5×10^{-4}), and the LRG high-entropy ceramic exhibits the nearest zero τ_f. Li-containing olivine microwave dielectric ceramics (such as $LiLuGeO_4$ and $LiYGeO_4$) usually possess a large $|\tau_f|$, primarily because of their large oxygen octahedral distortion. The distortion of oxygen octahedra in such microwave dielectric ceramics can be reduced by high-entropy ceramic synthesis, to achieve a stable temperature coefficient of resonant frequency.

In LTCC applications, the low sintering temperature and compatibility with Ag are essential for microwave dielectric ceramics. Because the sintering temperature of the LRG high-entropy ceramic is higher than the melting point of Ag, the sintering temperature should be lowered first. H_3BO_3 is a common sintering aid with a low melting point that reduces the sintering temperature of ceramics [8, 36-38]. Therefore, we added 3 wt.% H_3BO_3 to LRG and list the microwave dielectric properties (ε_r = 7.6, $Q\times f$ = 11700 GHz, and τ_f = −7.4 ppm/°C, sintered at 900 °C) of LRG + 3 wt.% H_3BO_3 ceramics in Table S2 (Supporting Information). The LRG + 3 wt.% H_3BO_3 high-entropy ceramic can be densified at 900 °C, and no secondary phases were observed in the XRD pattern (Fig. 4). This result indicates that the liquid phase of B_2O_3 was uncrystallized and distributed in the grain boundary as an amorphous state (Fig. S2, Supporting Information). The XRD pattern, backscattered electron (BSE) image, and EDS analysis of the LRG + 3 wt.% H_3BO_3 + 15 wt.% Ag sample that was cofired at 900 °C for 4 h

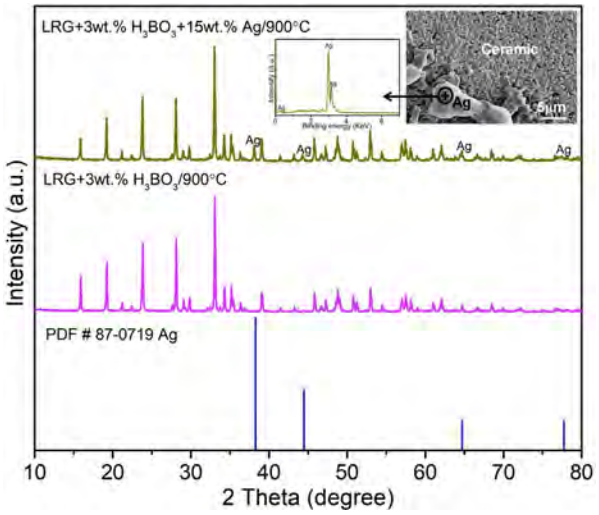

Fig. 4. XRD patterns of LRG + 3 wt.% H_3BO_3 and LRG + 3 wt.% H_3BO_3 + 15 wt.% Ag high-entropy ceramics sintered at 900 °C for 4 h. Inset shows backscattered electron image of LRG + 3 wt.% H_3BO_3 + 15 wt.% Ag ceramic.

are shown in Fig. 4. Only diffraction peaks of LRG and Ag were detected in the XRD patterns, and the LRG high-entropy ceramic was well-matched with Ag from the BSE image and EDS analysis.

4. Conclusions

We prepared a new olivine high-entropy ceramic $Li(Gd_{0.2}Ho_{0.2}Er_{0.2}Yb_{0.2}Lu_{0.2})GeO_4$ material via a facile solid-state reaction approach. When used as a microwave dielectric ceramic for LTCC technologies, the LRG high-entropy ceramic exhibited outstanding microwave dielectric properties, and delivered a stable τ_f of −2.9 ppm/°C. The five cations, Gd^{3+}, Ho^{3+}, Er^{3+}, Yb^{3+}, and Lu^{3+}, occupied the [RO_6] octahedron position, which affected the oxygen octahedron distortion. The [RO_6] octahedron with less distortion corresponded to the more stable temperature coefficient of the resonant frequency. The LRG high-entropy ceramic that was doped with 3 wt% H_3BO_3 provided several favorable features, such as a low sintering temperature (900 °C); a good chemical compatibility with silver; and microwave dielectric properties of $\varepsilon_r = 7.6$, $Q \times f = 11700$ GHz, and $\tau_f = -7.4$ ppm/°C. These characters enabled the LRG high-entropy ceramic to be a promising candidate for LTCC.

Declaration of competing interest

The authors declare that they have no known competing financial interests or personal relationships that could have appeared to influence the work reported in this paper.

Supporting information

Fig. S1. Crystal structure and refined XRD pattern of $LiLuGeO_4$ ceramic ($R_p = 7.25\%$, $R_{wp} = 10.3\%$, and $R_{exp} = 3.67\%$).

Fig. S2. SEM image of LRG + 3 wt.% H_3BO_3 high-entropy ceramics sintered at 900 °C for 4 h.

Table S1. Refined atomic fractional coordinates from XRD data for the $LiLuGeO_4$ sample and lattice parameters are $a = 11.1401(5)$ Å, $b = 6.3333(6)$ Å, $c = 5.0656(1)$ Å with a space group of *Pnma*.

Table S2. Microwave dielectric properties of LRG + 3 wt.% H_3BO_3 high-entropy ceramics sintered at different temperatures.

Acknowledgments

The authors gratefully acknowledge the financial support from the Shenzhen Basic Research General Program (No. JCYJ20190808114618998).

Supplementary materials

Supplementary material associated with this article can be found, in the online version, at doi:10.1016/j.jmst.2021.03.057.

References

[1] D. Wang, S. Zhang, G. Wang, Y. Vardaxoglou, W. Whittow, D. Cadman, D. Zhou, K. Song, I.M. Reaney, Appl. Mater. Today 18 (2020) 100519.
[2] H.H. Guo, D. Zhou, W.F. Liu, L.X. Pang, D.W. Wang, J.Z. Su, Z.M. Qi, J. Am. Ceram. Soc. 103 (2020) 423–431.
[3] P.S. Pálvölgyi, M. Nelo, O. Pitkänen, J. Peräntie, H. Liimatainen, S. Myllymäki, H. Jantunen, K. Kordas, Nanotechnology 31 (2020) 435203.
[4] T. Joseph, M.T. Sebastian, Mater. Lett. 65 (2011) 891–893.
[5] K.X. Song, X.M. Chen, X.C. Fan, J. Am. Ceram. Soc. 90 (2007) 1808–1811.
[6] C.X. Chen, S.P. Wu, Y.X. Fan, J. Alloys Compd. 578 (2013) 153–156.
[7] Y. Tang, M. Xu, L. Duan, J. Chen, C. Li, H. Xiang, L. Fang, J. Eur. Ceram. Soc. 39 (2019) 2354–2359.
[8] H. Xiang, C. Li, H. Jantunen, L. Fang, A.E. Hill, ACS Sustainable Chem. Eng. 6 (2018) 6458–6466.
[9] C. Li, H. Xiang, M. Xu, Y. Tang, L. Fang, J. Eur. Ceram. Soc. 38 (2018) 1524–1528.
[10] K. Cheng, C. Li, H. Xiang, Y. Sun, L. Fang, Mater. Lett. 228 (2018) 96–99.
[11] A. Sunny, K.A. Lazer, K.M. Manu, K.P. Surendran, M.T. Sebastian, J. Alloys Compd. 552 (2013) 83–87.
[12] C. Wu, Y. Hu, S. Bao, G. Wang, P. Jiang, J. Chen, Z. Duan, W. Deng, RSC Adv. 10 (2020) 29835.
[13] B.J. Tao, W.F. Wang, H.Y. Liu, T.X. Du, H.T. Wu, C.F. Xing, D.Z. Wang, Y.P. Zhang, Ceram. Int. 47 (2021) 2584–2590.
[14] L.T. Zhang, Y.J. Duan, T. Wada, H. Kato, J.M. Pelletier, D. Crespo, E. Pineda, J.C. Qiao, J. Mater. Sci. Technol. 83 (2021) 248–255.
[15] R.Z. Zhang, M.J. Reece, J. Mater. Chem. A 7 (2019) 22148.
[16] D.B. Miracle, Nat. Commun. 10 (2019) 1805.
[17] R. Feng, P.K. Liaw, M.C. Gao, M. Widom, NPJ Comput. Mater. 3 (2017) 50.
[18] C. Oses, C. Toher, S. Curtarolo, Nat. Rev. Mater. 5 (2020) 295–309.
[19] X. Yan, L. Constantin, Y. Lu, J.F. Silvain, M. Nastasi, B. Cui, J. Am. Ceram. Soc. 101 (2018) 4486–4491.
[20] J.W. Yeh, Ann. Chim. Sci. Mater. 31 (2006) 633–648.
[21] Y. Zhou, B. Zhao, H. Chen, H. Xiang, F.Z. Dai, S. Wu, Xue W, J. Mater. Sci. Technol. 74 (2021) 105–118.
[22] Y.L. Aung, S. Nakayama, M. Sakamoto, J. Mater. Sci. 40 (2005) 129–133.
[23] H.M. Rietveld, J. Appl. Crystallogr. 2 (1969) 65–71.
[24] B.W. Hakki, P.D. Coleman, IRE Trans Microwave Theory Technol 8 (1960) 402–410.
[25] A.J. Bosman, E.E. Havinga, Phys. Rev. 129 (1963) 1593–1600.
[26] I.D. Brown, R.D. Shannon, Acta Crystallogr. A 29 (1973) 266–282.
[27] R.D. Shannon, J. Appl. Phys. 73 (1993) 348–366.
[28] P.V. Rysselberghe, J. Phys. Chem. 36 (1932) 1152–1155.
[29] D. Zhou, H.H. Guo, M.S. Fu, X.G. Yao, H.X. Lin, W.F. Liu, L.X. Pang, C. Singh, S. Trukhanov, A. Trukhanov, I.M. Reaney, Inorg. Chem. Front. 8 (2021) 156–163.
[30] X.Q. Song, Z.Y. Zou, W.Z. Lu, T. Chen, S.W. Ta, Z.X. Fu, W. Lei, J. Alloys Compd. 835 (2020) 155340.
[31] J. Li, X.K. Lan, K. Du, X.Q. Song, W.Z. Lu, G.F. Fan, W. Lei, J. Am. Ceram. Soc. 102 (2019) 7480–7490.
[32] L.T. Liu, Y.G. Chen, Z.B. Feng, H.T. Wu, X.Y. Zhang, Ceram. Int. 47 (2021) 4321–4326.
[33] J. Chen, Y. Tang, M. Yu, C. Yin, Z. Zhang, H. Xiang, C. Li, X. Xing, L. Fang, Ceram. Int. 46 (2020) 4197–4203.
[34] C. Pei, J. Tan, Y. Li, G. Yao, Y. Jia, Z. Ren, P. Liu, H. Zhang, J. Adv. Ceram. 9 (2020) 588–594.
[35] E.S. Kim, D.H. Kang, IEEE Trans. Ultrason. Ferroelectr. Freq. Control. 55 (2008) 1069–1074.
[36] H.H. Guo, M.S. Fu, D. Zhou, C. Du, P.J. Wang, L.X. Pang, W.F. Liu, A.S.B. Sombra, J.Z. Su, ACS Appl. Mater. Interfaces 13 (2021) 912–923.
[37] H. Xiang, Y. Bai, J. Varghese, C. Li, L. Fang, H. Jantunen, J. Am. Ceram. Soc. 102 (2019) 1218–1226.
[38] H.I. Hsiang, C.C. Chen, S.Y. Yang, J. Adv. Ceram. 8 (2019) 345–351.
[39] C. Su, L. Ao, Z. Zhang, Y. Zhai, J. Chen, Y. Tang, L. Liu, L. Fang, Ceram. Int. 46 (2020) 19996–20003.